Acta Materialia 205 (2021) 116578

Contents lists available at ScienceDirect

Acta Materialia

journal homepage: www.elsevier.com/locate/actamat

Acta Materialia

Isovalent sulfur substitution to induce a simultaneous increase in the effective mass and weighted mobility of a *p*-type Bi-Sb-Te alloy: an approach to enhance the thermoelectric performance over a wide temperature range

Kyu Hyoung Lee[a,†], Hyun-Sik Kim[b,†], Minyoung Kim[a], Jong Wook Roh[c], Jae-Hong Lim[d], Won Joong Kim[e], Sang-il Kim[e,*], Wooyoung Lee[a,*]

[a] Department of Materials Science and Engineering, Yonsei University, Seoul 03722, South Korea
[b] Department of Materials Science and Engineering, Hongik University, Seoul 04066, South Korea
[c] School of Nano & Materials Science and Engineering, Kyungpook National University, Sangju 37224, South Korea
[d] Department of Materials Science and Engineering, Gachon University, Seongnam 13120, South Korea
[e] Department of Materials Science and Engineering, University of Seoul, Seoul 02504, South Korea

ARTICLE INFO

Article history:
Received 19 October 2020
Revised 15 December 2020
Accepted 15 December 2020
Available online 18 December 2020

Keywords:
thermoelectric
Bi-Sb-Te
bipolar
effective mass
weighted mobility

ABSTRACT

A significant obstacle to obtaining enhanced thermoelectric performance (defined by a thermoelectric figure of merit, zT) in commercial *p*-type Bi-Sb-Te alloys is bipolar transport originating from their intrinsic narrow-band-gap semiconducting characteristics. Cation-site doping is commonly used to suppress the bipolar conduction. However, zT enhancement occurs often only at elevated temperatures since the electronic thermal conductivity mainly increases at low temperatures due to the increase of hole concentration. Herein, the substitution of isovalent S ions in the anion Te-site of Bi-Sb-Te is explored to obtain a high zT over a wide temperature range by simultaneously increasing the density-of-states effective mass and weighted mobility. The zT of $Bi_{0.49}Cu_{0.01}Sb_{1.5}Te_3$ is enhanced by ~10 % for all measured temperatures, and the average zT increases beyond 1.0 between 300 and 520 K, benefitting from the synergetic control of band structure and deformation potential via S substitution.

1. Introduction

In the current energy crisis and the era of climate change, many industrial and general applications continue to unavoidably generate huge amounts of waste heat. Two-thirds of the waste heat is low-grade with temperatures below 200°C [1]. Therefore, recovering low-grade waste heat is an important challenge in improving energy usage efficiency. Thermoelectric power generation (TEG) is a key technology for converting waste heat into electric energy. The energy conversion efficiency of TEG system is directly determined by the performance of thermoelectric materials and is evaluated via a dimensionless figure of merit, zT ($= S^2 \cdot \sigma \cdot T/\kappa_{tot}$, where S, σ, T, and κ_{tot} are the Seebeck coefficient, electrical conductivity, absolute temperature, and total thermal conductivity, respectively). Thus, most research on commercial thermoelectric materials has focused on the increase in zT values by enhancing the power factor ($S^2 \cdot \sigma$) and/or reducing κ_{tot}.

The average zT (zT_{avg}) between the operating temperatures is more critical than the maximum zT (zT_{max}) to achieve the maximum energy conversion efficiency, η_{max}, as shown by the following equation:

$$\eta_{max} = \frac{\Delta T}{T_h} \frac{\sqrt{1+zT_{avg}} - 1}{\sqrt{1+zT_{avg}} + \frac{T_c}{T_h}} \quad (1)$$

where T_c is the cold-side temperature, T_h is the hot-side temperature, ΔT is ($T_h - T_c$), and T_{avg} is ($T_h + T_c$)/2.

For a low-grade heat TEG system, Bi_2Te_3-based alloys are the only commercial option, exhibiting the highest zT between room temperature and 200 °C [2]. To secure economic feasibility by improving η_{max}, many efforts have been made to enhance their zT. For example, cation-site doping with Pb, Ag, and Cu in *p*-type $(Bi,Sb)_2Te_3$-based alloys has been effective for enhancing zT; this is mainly because of the suppressed bipolar thermal conduction benefitting from an increase in majority hole carriers [3–8]. How-

* Correspondence authors
E-mail addresses: sang1.kim@uos.ac.kr (S.-i. Kim), wooyoung@yonsei.ac.kr (W. Lee).
† These authors contributed equally to this work

https://doi.org/10.1016/j.actamat.2020.116578
1359-6454/

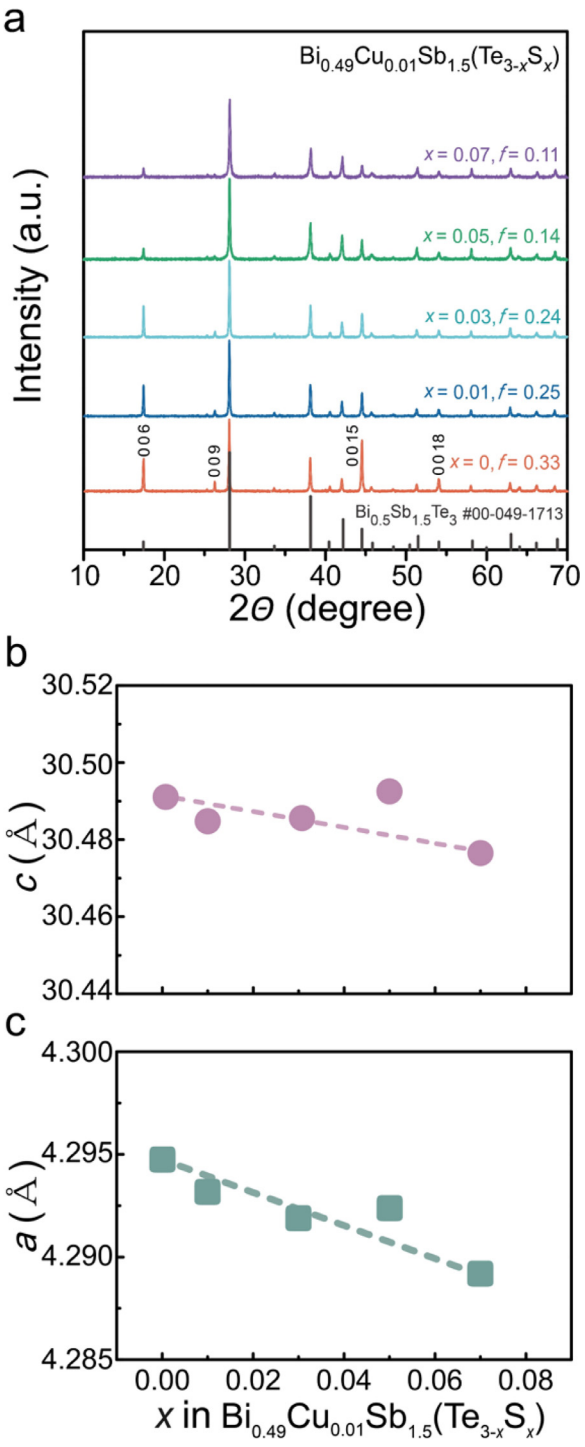

Fig. 1. (a) X-ray diffraction patterns and calculated lattice parameters (b) *c* and (c) *a* of the $Bi_{0.49}Cu_{0.01}Sb_{1.5}(Te_{3-x}S_x)$ samples.

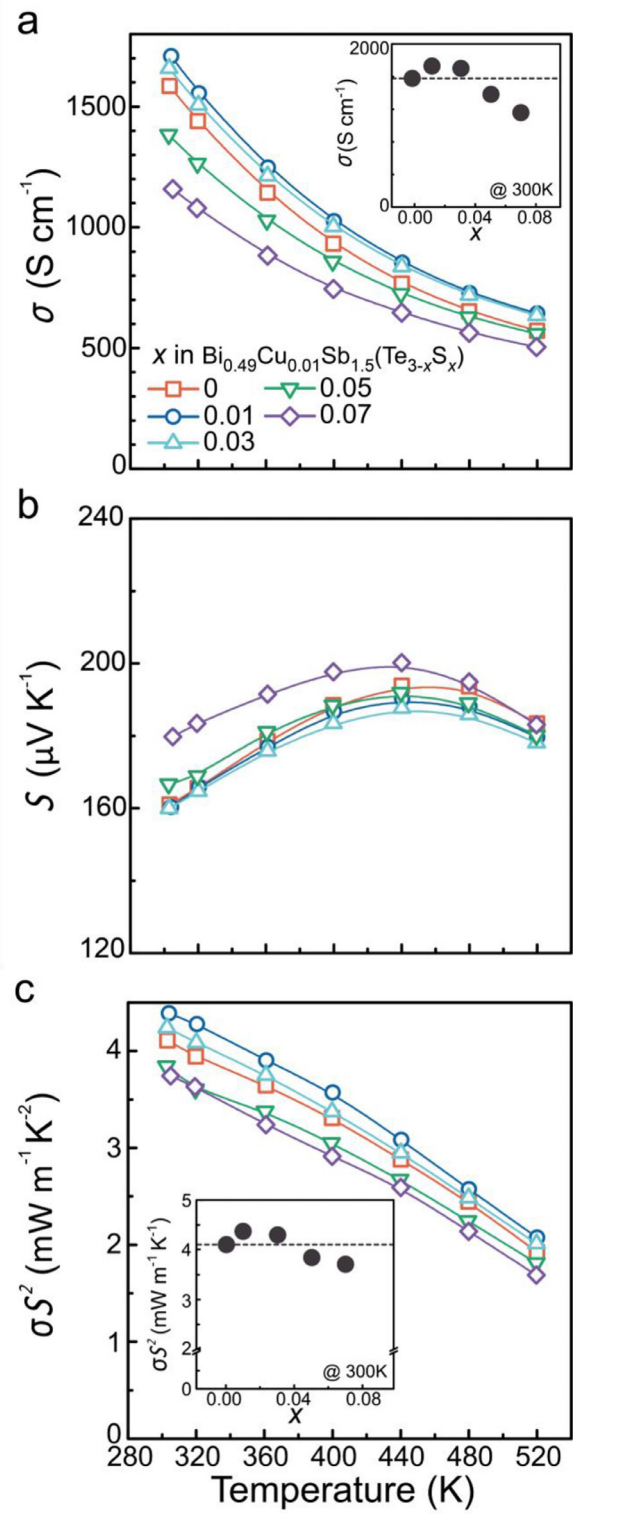

Fig. 2. Temperature-dependent (a) electrical conductivity, σ, (b) Seebeck coefficient, *S*, and (c) power factor of $Bi_{0.49}Cu_{0.01}Sb_{1.5}(Te_{3-x}S_x)$ samples. The inset of (c) shows the power factor at 300 K according to the S substitution content.

ever, the effect of reducing bipolar thermal conduction is only valid at elevated temperatures because, in Bi_2Te_3-based alloys, the bipolar thermal conductivity (κ_{bp}) only increases at high temperatures; the electronic thermal conductivity (κ_{elec}) largely increases across all temperatures, owing to the increased hole concentration from *p*-type doping. Thus, the maximum temperature of *zT* increases; however, the enhancement of zT_{avg} is rather constrained. Other cation substitutions—with Al, Ga, In, and Fe—also showed a similar trend [9–12].

Many nanostructure-based approaches have been demonstrated as effective methods of enhancing zT_{avg} [13–16]; however, a simple and efficient compositional tuning route is always more favorable for reproducible mass-scale production. The remaining challenges in Bi-Sb-Te alloys based on compositional tuning is in Te-site substitution and in the development of advanced concepts beyond the

Table 1
Band parameters obtained using a two-band model at room temperature.

$Bi_{0.49}Cu_{0.01}Sb_{1.5}(Te_{3-x}S_x)$		$x = 0$	$x = 0.01$	$x = 0.03$	$x = 0.05$	$x = 0.07$
Valence band (VB)	VB E_{def} (eV)	13.87	13.28	13.44	13.92	13.40
	VB m_d^* (m_0)	1.14	1.17	1.17	1.23	1.35
	VB μ_0 ($cm^2V^{-1}s^{-1}$)	324.5	333.8	323.7	270.0	225.9
	U_{VB} ($cm^2V^{-1}s^{-1}$)	395.0	419.8	410.2	366.1	354.4
	Hole concentration (cm^{-3})	4.20×10^{19}	4.40×10^{19}	4.40×10^{19}	4.34×10^{19}	4.21×10^{19}
Conduction band (CB)	CB E_{def} (eV)	10.90	11.54	11.74	12.16	12.98
	CB m_d^* (m_0)	0.83	0.83	0.83	0.83	0.83
	CB μ_0 ($cm^2V^{-1}s^{-1}$)	186.2	165.4	160.8	150.1	130.1
	U_{CB} ($cm^2V^{-1}s^{-1}$)	140.8	125.0	121.6	113.5	98.44
	Electron concentration (cm^{-3})	3.46×10^{16}	3.48×10^{16}	3.38×10^{16}	3.78×10^{16}	5.18×10^{16}

previous approach of bipolar transport suppression by increasing the majority carrier concentration.

In the present study, we demonstrate that the substitution of isovalent S at the Te-site of *p*-type Bi-Sb-Te alloys allows the simultaneous improvement of S and σ. Cu-doped Bi-Sb-Te, $Bi_{0.49}Cu_{0.01}Sb_{1.5}Te_3$, was selected as the reference material, and polycrystalline bulks of S-substituted $Bi_{0.49}Cu_{0.01}Sb_{1.5}Te_3$ were prepared. To elucidate the effect of the S substitution on the electronic transport properties of $Bi_{0.49}Cu_{0.01}Sb_{1.5}Te_3$, physical parameters, such as density-of-states effective mass (m_d^*), deformation potential (E_{def}), and weighted mobility (U), were evaluated. Interestingly, m_d^* and U for hole carriers increased simultaneously up to ~1 at.% S substituted samples. The analysis based on a two-band model connected with a single parabolic band (SPB) model indicates that modifying the electronic structure includes band structure modification for enlarged S and lowered E_{def} for improved σ. Hence, the isovalent S substitution at the Te-site enables zT enhancement in *p*-type $Bi_{0.49}Cu_{0.01}Sb_{1.5}Te_3$ by ~ 10% at all temperatures, and the zT_{avg} value in a wide temperature range of 300–520 K reaches above 1.0.

2. Experimental

High-purity (> 99.99%) Bi, Sb, Te, Cu, and S granules and powders were weighed with compositions of pristine $Bi_{0.49}Cu_{0.01}Sb_{1.5}Te_3$ and a series of S-substituted $(Bi_{0.49}Cu_{0.01}Sb_{1.5})(Te_{3-x}S_x)$ (x = 0.01, 0.03, 0.05, and 0.07). Properly weighed raw elemental materials were loaded into a quartz tube (14 mm in diameter) with a carbon-coated inner wall via acetone cracking and vacuum sealed at 10^{-3} Torr. The ingots were then prepared by a conventional melt-solidification process (melted at 1423 K for 20 h and water quenched). Powders were obtained from the ingots by high-energy ball milling (8000M Mixer/Mill, SPEX SamplePrep, Metuchen, NJ, USA) for 10 min, and compacted bulks (~10 mm in diameter and ~13 mm in thickness) were fabricated by spark plasma sintering (SPS) at 703 K and 60 MPa for 5 min. The densities (ρ_s) of the SPSed bulks, measured by Archimedes' principle (MD-300S, Alfa Miracle, Japan), were > 97 % of the theoretical densities. The phase formation behavior and crystal orientation of the SPSed bulks were analyzed by X-ray diffraction (XRD, SmartLab, Rigaku, Japan) with CuKα radiation (λ = 1.5418 Å).

To measure S, σ, and κ_{tot} in the same direction (perpendicular to the SPS press direction), a rectangular bar-type sample (8 mm × 3 mm × 3 mm) for the measurement of S and σ and a square plate-type sample (10 mm × 10 mm × 1 mm) for the measurement of thermal diffusivity (D) were cut in a plane perpendicular and parallel to the SPS press direction, respectively. The temperature-dependent S and σ were measured over the temperature range of 300–520 K, under a He atmosphere using a commercial measurement system (ZEM-3 Advanced-RIKO, Yokohama, Japan). The carrier concentrations were determined by Hall measurements in the van der Pauw configuration in a magnetic field of 0.5 T (AHT-55T5, Ecopia, Anyang, South Korea). The κ_{tot} ($= \rho_s \cdot C_p \cdot D$) values of the samples were calculated from the separate measurements of ρ_s, heat capacity (C_p), and D. The C_p values according to temperature were obtained via the thermal relaxation method from 100 to 400 K using a Quantum Design physical properties measurement system, and the temperature-dependent C_p was estimated from 300 to 520 K based on the Dulong-Petit fitting. Temperature-dependent D was measured by the laser flash method (TC-1200RH, Ulvac-Riko, Japan) from 300 to 520 K under vacuum.

3. Results and Discussion

Fig. 1(a) shows the XRD patterns of the SPSed S-substituted $(Bi_{0.49}Cu_{0.01}Sb_{1.5})(Te_{3-x}S_x)$ (x = 0, 0.01, 0.03, 0.05, and 0.07) bulks. All samples show a single phase of Bi-Sb-Te (#00-049-1713 for $Bi_{0.5}Sb_{1.5}Te_3$), without any S-related impurities. The lattice parameters c and a were calculated from XRD (Figs. 1(b) and 1(c)), revealing that both the a and c parameters decreased gradually with increasing S substitution due to the difference in the ionic radii between S^{2-} (170 pm) and Te^{2-} (207 pm). This systematic change in the lattice parameters provides further evidence for the S substitution at the Te-site. It should be noted that the 00*l*-orientation, which is generally evaluated by the Lotgering factor f ($f_{00l} = (p_{00l} - p_0)/(1 - p_0)$, where $p_{00l} = \Sigma I_{00l}/\Sigma I_{hkl}$ and $p_0 = \Sigma I^0_{00l}/\Sigma I^0_{hkl}$, with I_{hkl} and I^0_{hkl} being the intensities of *the (h k l)* peaks for the textured and randomly oriented samples) [17] decreased with increasing substituted S content due to the rigid bonding characteristics originating from the larger electronegativity of S (χ_S = 2.58) compared to that of Te (χ_{Te} = 2.1).

The measured temperature-dependent σ and S values are shown in Figs. 2(a) and 2(b). The σ value of the pristine sample ($Bi_{0.49}Cu_{0.01}Sb_{1.5}Te_3$) at 300 K was 1585 S cm^{-1} and increased to 1708 S cm^{-1} for $Bi_{0.49}Cu_{0.01}Sb_{1.5}Te_{2.99}S_{0.01}$ (x = 0.01), as shown in the inset of Fig. 2(a). After exhibiting a maximum σ at x = 0.01, σ gradually decreased with the increasing content of substituted S. Conversely, the S value of the pristine sample at 300 K was 161 μV K^{-1} and remained almost unchanged up to x = 0.03 (Fig. 2(b))—which is clearly different from the behavior observed in the cation (Pb, Ag, Cu)-doped Bi-Sb-Te alloys [3–8]—then gradually increased to 193 μV K^{-1} for x = 0.07. To clarify this, we evaluated the Hall carrier concentration (n_H) and Hall mobility (μ_H) at 300 K, as shown in Fig. 3(a). The value of n_H did not change much with the content of substituted S as the isovalent S substitution in the Te-site would not generate any carriers. A slight increase in the n_H value upon S substitution from 4.2×10^{19} (x = 0) to ~4.4×10^{19} cm^{-3} (x = 0.01 and x = 0.03) is considered to be related to the suppression of antisite defect formation, which suppresses the elimination of holes. However, the μ_H values of x = 0.01 (~246 cm^2 V^{-1} s^{-1}) and x = 0.03 (~236 cm^2 V^{-1} s^{-1}) samples are rather high compared to those of the pristine sample (~237 cm^2 V^{-1} s^{-1}),

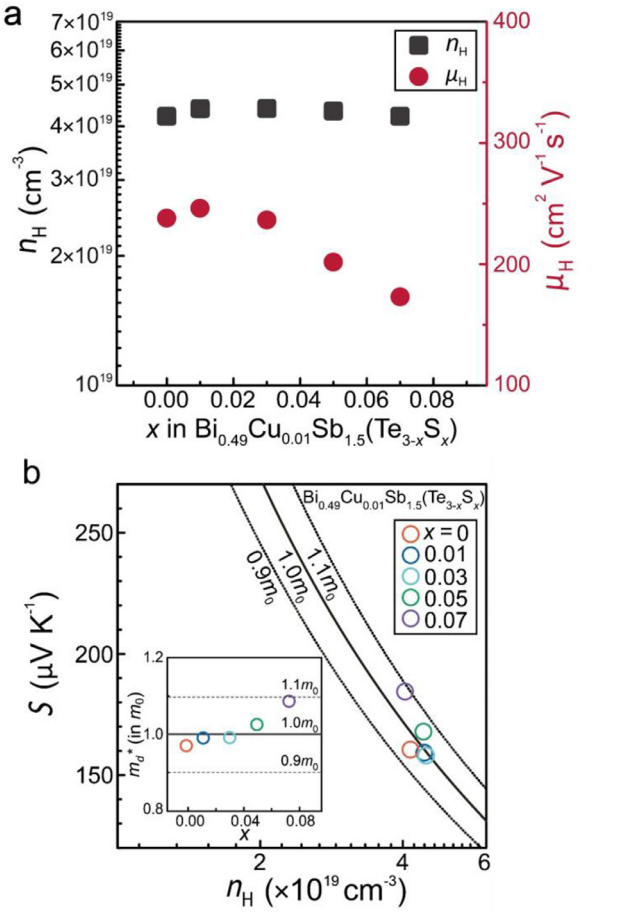

Fig. 3. (a) Estimated carrier concentrations and mobilities of $Bi_{0.49}Cu_{0.01}Sb_{1.5}(Te_{3-x}S_x)$ samples according to the S substitution content. (b) Pisarenko plot of $Bi_{0.49}Cu_{0.01}Sb_{1.5}(Te_{3-x}S_x)$ samples at 300 K. The inset of (b) shows the density-of-states effective mass (m_d*) values at 300 K.

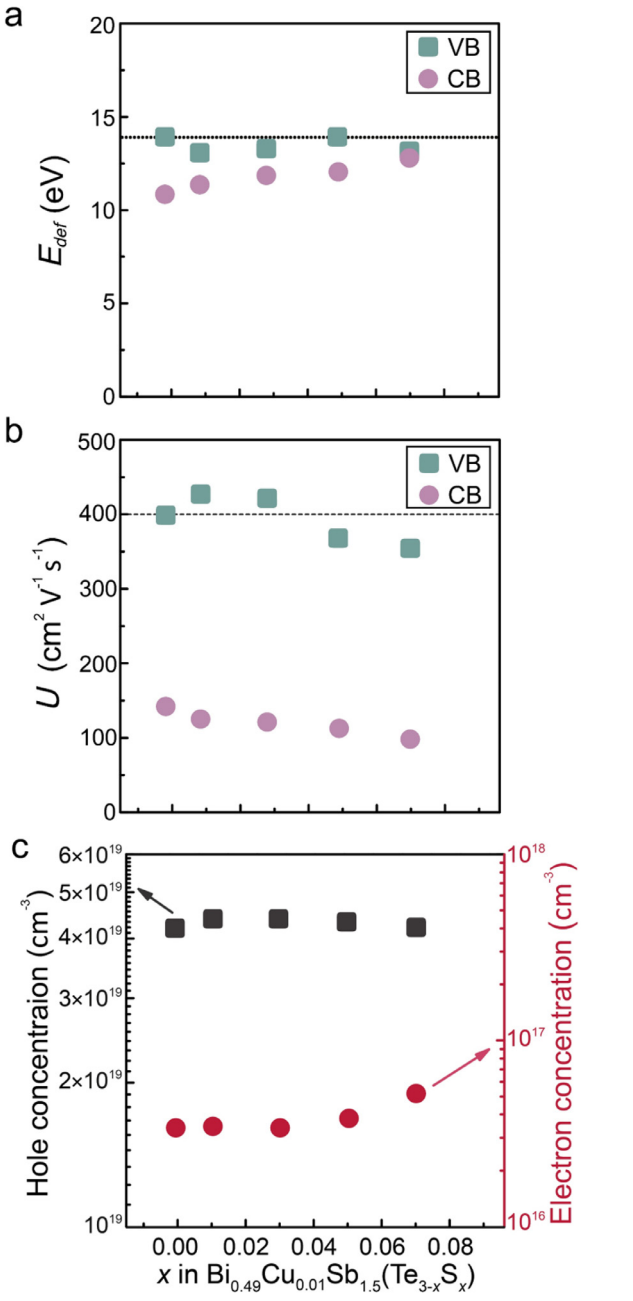

Fig. 4. (a) Hole and electron concentrations, (b) deformation potentials, and (c) weighted mobilities for valence and conduction bands of the $Bi_{0.49}Cu_{0.01}Sb_{1.5}(Te_{3-x}S_x)$ samples according to the S substitution content.

despite the lower 00*l*-orientation (Fig. 1(a)). Thus, the origin of the higher σ values observed in the $x = 0.01$ and $x = 0.03$ samples are attributed to the simultaneous improvement of n_H and μ_H. This synergetic effect, as shown in Fig. 2(c) and the inset of Fig. 2(c), results in the power factor values (~3.64 mW m^{-1} K^{-2} for pristine $Bi_{0.49}Cu_{0.01}Sb_{1.5}Te_3$) at 300 K further increasing to ~4.39 mW m^{-1} K^{-2} for $x = 0.01$ and ~3.94 mW m^{-1} K^{-2} for $x = 0.03$ samples, entirely due to the increase in σ while maintaining S. This implies improved hole transport characteristics, which are directly related to the modification of the electronic structure by S substitution.

m_d* is an important parameter to confirm the electronic structure modification and hence we provided a Pisarenko plot (S as a function of n_H) at 300 K, as shown in Fig. 3(b); the solid line represents S for m_d* of 1.0 m_0 (where m_0 is the free electron mass) and the dotted lines correspond to S values for m_d* of 0.9 and 1.1 m_0, via the following equation:

$$S = \frac{8\pi^2 k_B^2}{3eh^2}\left(\frac{\pi}{3n_H}\right)^{2/3} m_d^* T, \quad (2)$$

where e, h, and k_B are the elementary charge, Plank's constant, and Boltzmann constant, respectively. Interestingly, m_d* gradually increases with S substitution, indicating that the electronic structure of the valence band (VB) of $Bi_{0.49}Cu_{0.01}Sb_{1.5}Te_3$ is modified, which is favorable for *p*-type transport. The inset of Fig. 3(b) shows the m_d* values with the content of substituted S. By considering the bipolar conduction behavior of Bi-Sb-Te alloys, quantitative analysis using the two-band model based on the SPB was conducted to investigate the band parameters for both the VB and CB, as presented in Table 1. The individual electrical conductivities (σ_i) and Seebeck coefficients (S_i) for VB and CB (where $i = p$ and n for the VB and CB, respectively) are fitted to the experimentally measured total σ and S using the following equation:

$$\sigma = \sigma_p + \sigma_n \quad (3)$$

$$S = \frac{\sigma_p S_p - \sigma_n S_n}{\sigma_p + \sigma_n} \quad (4)$$

Subsequently, using the SPB model, the E_{def} and effective mass (m_d*) values for the VB and CB were fitted to the total S and σ [18]. For calculation, we considered the valley degeneracies (N_v) of the VB and CB to be equal to 2 and 6, respectively, and a longitudinal elastic modulus (C_l) of 64.6 GPa, which was calculated from the

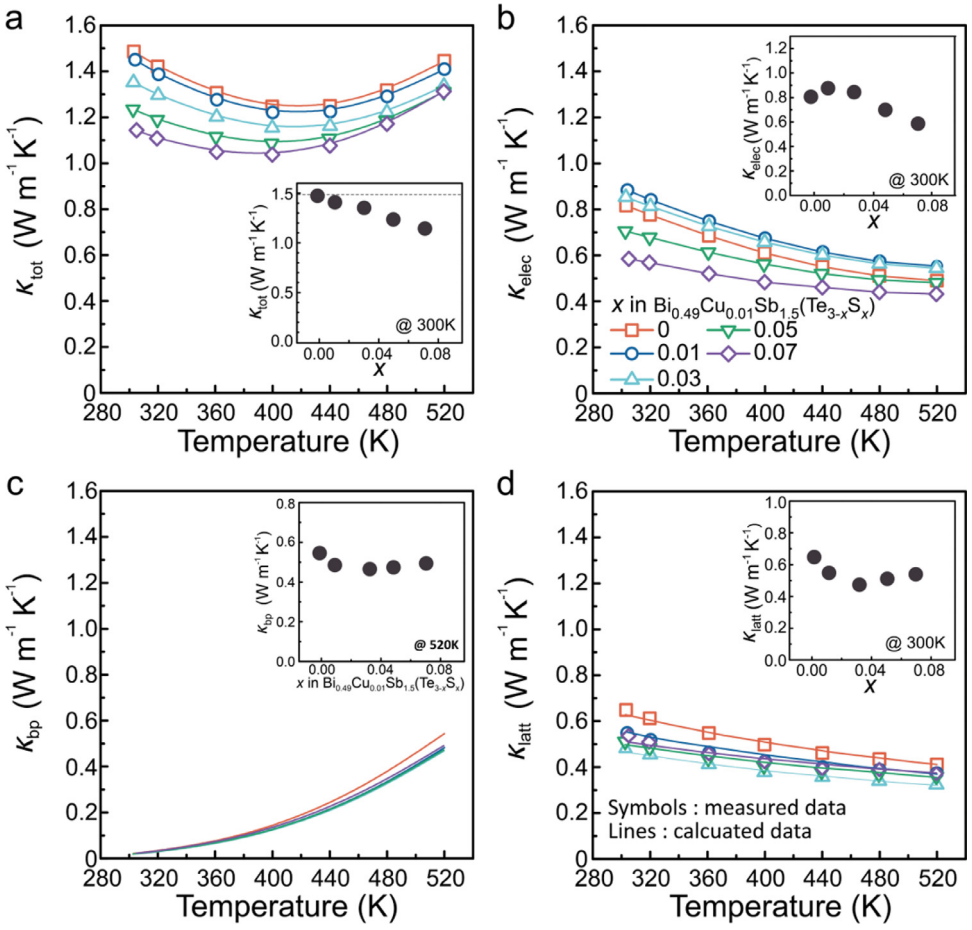

Fig. 5. Temperature-dependent (a) total thermal conductivity κ_{tot}, (b) electronic thermal conductivity κ_{elec}, (c) bipolar thermal conductivity κ_{bp}, and lattice thermal conductivity κ_{latt} of the $Bi_{0.49}Cu_{0.01}Sb_{1.5}(Te_{3-x}S_x)$ samples. The insets of (a)–(d) show the values at 300 K according to the S substitution content.

longitudinal speed of sound (v_l) and ρ_s of Bi_2Te_3 ($C_l = {v_l}^2 \cdot \rho_s$). In addition, the concentration of electrons and holes were calculated using the following equation:

$$R_{Htot} = \frac{R_{Hp}{\sigma_p}^2 + R_{Hn}{\sigma_n}^2}{(\sigma_p + \sigma_n)^2} \quad (5)$$

where R_{Htot}, R_{Hp}, and R_{Hn} are the Hall coefficients for the total conduction, VB, and CB, respectively; the R_{Hp} and R_{Hn} parameters were converted to hole and electron concentrations, respectively. E_{def} refers to the magnitude of the carrier–phonon interaction (hole–phonon and electron–phonon interactions in VB and CB, respectively), which is the perturbed charge carrier scattering induced by phonon waves. The non-degenerated mobility μ_0 is calculated for holes and electrons based on Eq. (6), which shows an inverse relationship with E_{def}.

$$\mu_0 = \frac{e\pi\hbar^4 C_l N_v^{\frac{5}{3}}}{\sqrt{2}E_{def}^2 {m_d^*}^{\frac{5}{2}} (k_B T)^{\frac{3}{2}}} \quad (6)$$

where ħ is Dirac's constant. In addition, U, which is a product of μ_0 and $({m_d}^*)^{3/2}$ ($U = \mu_0 \cdot ({m_d}^*)^{3/2}$) is then calculated for the holes and electrons, providing a quantitative comparison of how the changes in ${m_d}^*$ and E_{def} influence the charge transport together. As shown in Fig. 4(a), the E_{def} values of the VB for the $x = 0.01$ and $x = 0.03$ samples decrease to 13.28 eV and 13.44 eV compared to 13.87 eV for the pristine sample ($x = 0$), suggesting weakened phonon-hole interactions. However, a gradual increase in E_{def} of CB is observed, which indicates the intensified coupling between electrons and phonons by S substitution. Consequently, unexpected changes in U of the VB and CB, which is favorable for p-type conduction, is obtained by a small amount of S substitution, as shown in Fig. 4(b). The U of the VB improved from 395 $cm^2\ V^{-1}\ s^{-1}$ ($x = 0$) to 420 $cm^2\ V^{-1}\ s^{-1}$ for the $x = 0.01$ sample and 410 $cm^2\ V^{-1}\ s^{-1}$ for the $x = 0.03$ sample, while the U of the CB decreased. As shown in Table 1 and Fig. 4(b), a small amount of S substitution ($x = 0.01$ and 0.03) increased the band effective mass (${m_d}^*$) and U of the VB simultaneously. Fig. 4(c) shows the calculated hole and electron concentration with the content of the substituted S. Hole and electron concentrations do not change much up to $x = 0.03$, whereas the electron concentration increases with further S substitution, suggesting the generation of electrons by the formation of antisite defects.

Fig. 5(a) shows the temperature-dependent κ_{tot} for the S-substituted $Bi_{0.49}Cu_{0.01}Sb_{1.5}Te_3$ samples, showing that κ_{tot} gradually decreases with the increase in the content of the substituted S. At 300 K, the κ_{tot} of the pristine sample (~1.49 $W\ m^{-1}\ K^{-1}$) is reduced to ~1.14 $W\ m^{-1}K^{-1}$ for the $x = 0.07$ sample (inset of Fig. 5(a)). To understand the fundamentals of the change in κ_{tot}, we analyze the compositional contributions to the total thermal conduction, given by the following equation:

$$\kappa_{tot} = \kappa_{latt} + \kappa_{elec} + \kappa_{bp}, \quad (7)$$

where κ_{latt} is the lattice thermal conductivity. First, κ_{elec} was calculated using Wiedemann-Franz ($\kappa_{elec} = L \cdot \sigma \cdot T$, where L is the Lorenz number, details are described in the Supplemental Information). As shown in Fig. 5(b) and the inset of Fig. 5(b), a similar behavior to σ (Fig. 2(a) and the inset of Fig. 2(a)) is observed within the entire measured temperature range due to the negli-

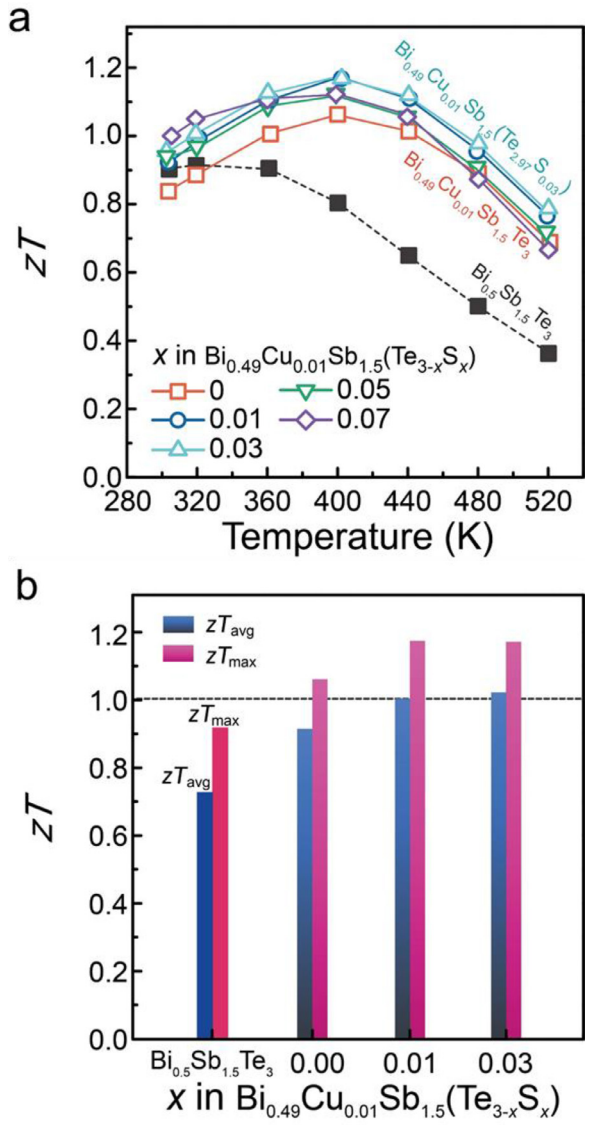

Fig. 6. (a) Dimensionless thermoelectric figure of merit (zT) as a function of temperature and (b) maximum zT (zT_{max}) and average zT (zT_{avg}) between 300 and 520 K according to the S substitution content of the $Bi_{0.49}Cu_{0.01}Sb_{1.5}(Te_{3-x}S_x)$ samples.

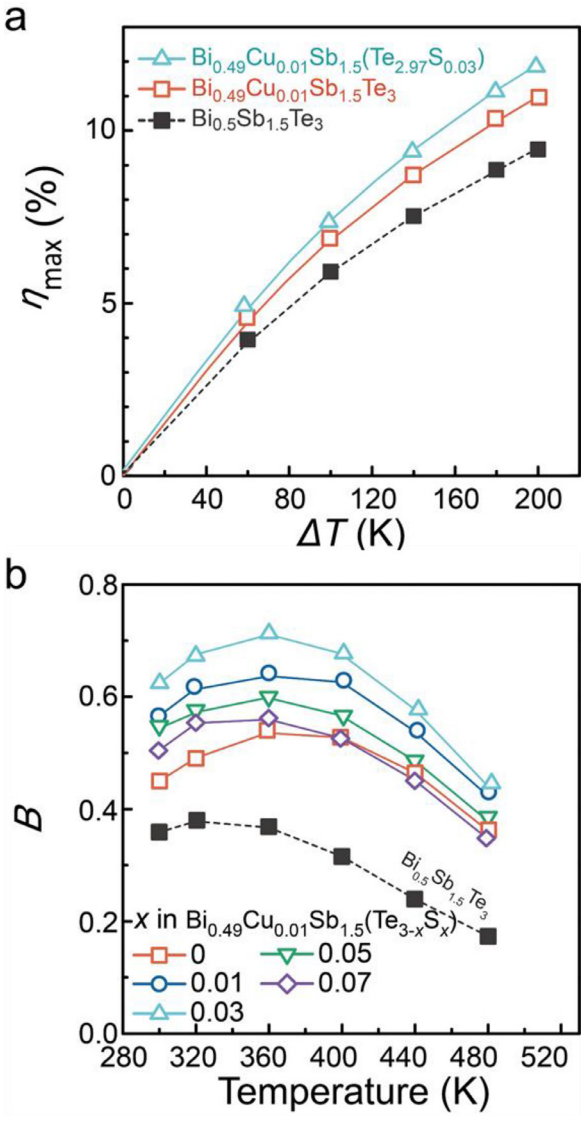

Fig. 7. (a) Maximum thermoelectric energy conversion efficiency (η_{max}) as a function of temperature difference (ΔT) and (b) temperature-dependent quality factor (B) of the $Bi_{0.49}Cu_{0.01}Sb_{1.5}(Te_{3-x}S_x)$ samples.

gible change in L with the content of substituted S. Second, κ_{bp}, shown in Fig. 5(c), is estimated using:

$$\kappa_{bp} = \left(S_p{}^2\sigma_p + S_n{}^2\sigma_n - S^2\sigma\right)T \tag{8}$$

At higher temperatures, the S substitution slightly reduces κ_{bp} by the activation of the p-type conduction. As shown in the inset of Fig. 5(c), κ_{bp} at 520 K of the pristine sample (~0.544 W m^{-1} K^{-1}) is reduced in values ranging from 0.468 – 0.497 W m^{-1} K^{-1} by the S substitution. It is noted that the mechanism of κ_{bp} reduction is related to the independent control of transport parameters for the VB and CB. The experimental κ_{latt} values are calculated by subtracting κ_{elec} and κ_{bp} from κ_{tot}, and are shown as symbols in Fig. 5(d). The theoretical κ_{latt} (lines in Fig. 5(d)) is estimated via the Debye-Callaway model as follows:

$$\kappa_{latt} = \frac{k_B}{2\pi^2 v}\left(\frac{k_B T}{\hbar}\right)^3 \int_0^{\theta_D/T} \frac{\tau_{tot}(z) z^4 e^z}{(e^z-1)^2} dz, \tag{9}$$

where v, Θ_D, and τ_{tot}, are the phonon group velocity, Debye temperature, and total phonon relaxation time, respectively, and $z = \hbar\omega/k_B T$ (ω = phonon frequency). The details of the calculation are described in the Supplemental Information. It is clearly observed that κ_{latt} is monotonically reduced up to $x = 0.03$, mainly due to the intensified point defect (substituted S at Te-site) phonon scattering. In contrast, κ_{latt} increases at higher S substitution contents, as clearly shown in the inset of Fig. 5(d) (κ_{latt} at 300 K as a function of the S substitution content). As observed from the XRD patterns, this is considered to be related to the rigid bonding characteristics originating from the large electronegativity of S.

Fig. 6(a) shows the temperature-dependent zT values of all samples. The values for $Bi_{0.5}Sb_{1.5}Te_3$ is also shown for comparison. The S substitution enhances the zT of $Bi_{0.49}Cu_{0.1}Sb_{1.5}Te_3$, and the highest zT of 1.17 at 400 K is obtained both in $Bi_{0.49}Cu_{0.01}Sb_{1.5}Te_{2.99}S_{0.01}$ and $Bi_{0.49}Cu_{0.01}Sb_{1.5}Te_{2.97}S_{0.03}$, owing to the simultaneous engineering of electronic and thermal transport properties. Compared with the pristine sample, zT is enhanced by over 10% at all measured temperatures by the S substitution for $Bi_{0.49}Cu_{0.01}Sb_{1.5}Te_{2.97}S_{0.03}$. The S substitution increases zT_{avg} and zT_{max}, and zT_{avg} between 300 K and 520 K increases beyond 1.0 for $x = 0.01$ and $x = 0.03$, as shown in Fig. 6(b). This proves that the substitution of an isovalent S allows zT enhancement at all temper-

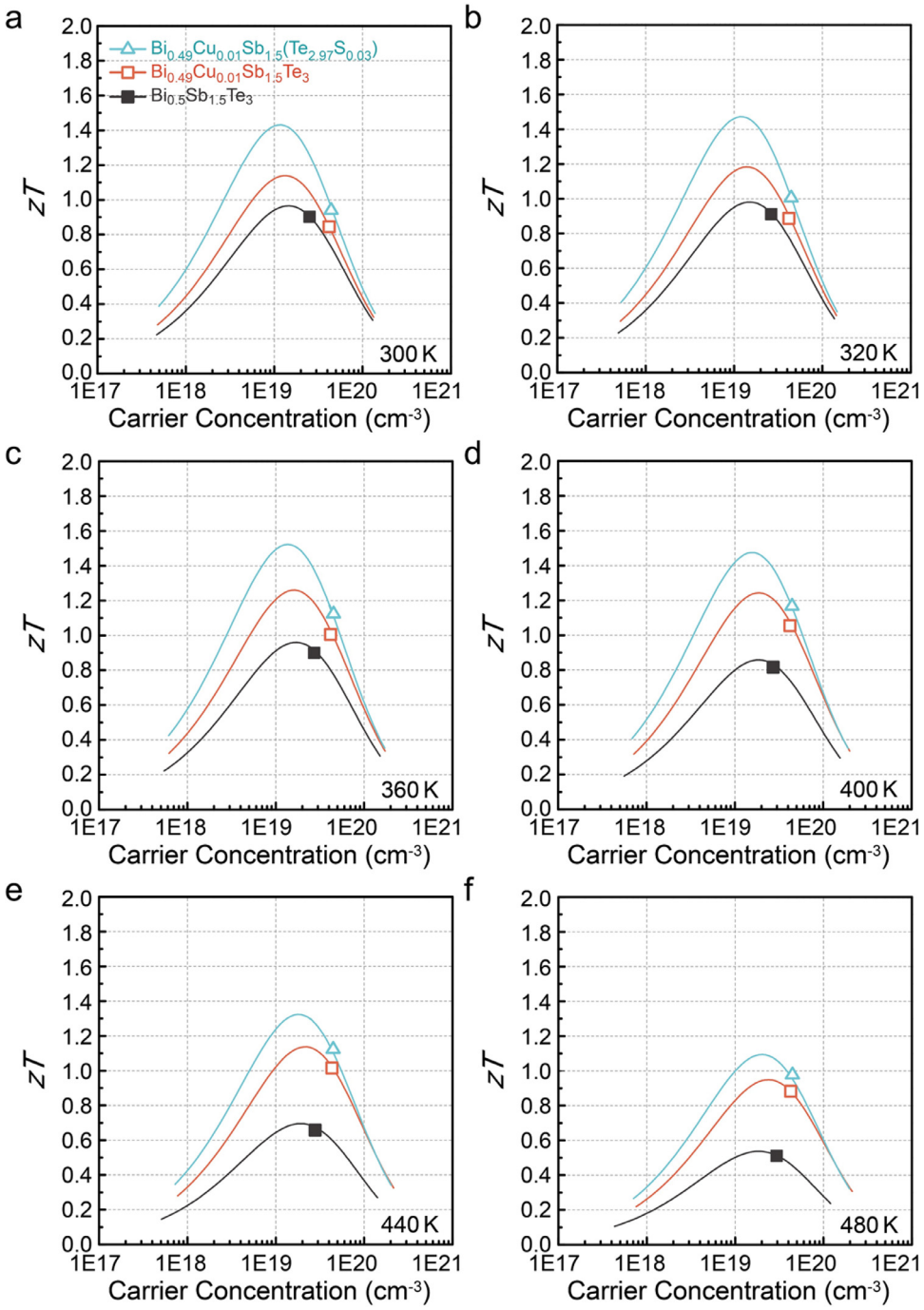

Fig. 8. Theoretical (solid lines) and experimental (symbols) zT as a function of the Hall carrier concentration for the $Bi_{0.5}Sb_{1.5}Te_3$, $Bi_{0.49}Cu_{0.01}Sb_{1.5}Te_3$, and $Bi_{0.49}Cu_{0.01}Sb_{1.5}Te_{2.97}S_{0.03}$ samples at various temperatures of (a) 300 K, (b) 320 K, (c) 360 K, (d) 400 K, (e) 440 K, and (f) 480 K.

atures by the favorable tuning of the electronic transport parameters (increased m_d^* and U of the VB) for p-type conduction.

η_{max} was calculated using Eq. (1) and compared for $Bi_{0.5}Sb_{1.5}Te_3$, $Bi_{0.49}Cu_{0.01}Sb_{1.5}Te_3$, and $Bi_{0.49}Cu_{0.01}Sb_{1.5}Te_{2.97}S_{0.03}$, as shown in Fig. 7(a). Benefiting from the simultaneous increase of zT_{avg} and zT_{max}, η_{max} is enhanced by 7.5% and 18.4 % at $\Delta T = 200$ K for $Bi_{0.49}Cu_{0.01}Sb_{1.5}Te_3$ and $Bi_{0.5}Sb_{1.5}Te_3$, respectively. Additionally, the quality factor (B factor) is calculated [18–20] based on the SPB model. The dimensionless B factor can be expressed using the following equation:

$$B = \frac{16\sqrt{2}\pi}{e}\frac{m_0^{3/2}k_B^{7/2}}{h^3}\mu_0\left(\frac{m_d^*}{m_0}\right)^{3/2}\frac{T^{5/2}}{\kappa_l}, \quad (10)$$

where κ_l is $\kappa_{tot} - \kappa_{elec}$. Therefore, in our analysis, κ_l is equivalent to $\kappa_{latt} + \kappa_{bp}$, so Eq. (9) is modified as:

$$B = \frac{16\sqrt{2}\pi}{e}\frac{m_0^{3/2}k_B^{7/2}}{h^3}\mu_0\left(\frac{m_d^*}{m_0}\right)^{3/2}\frac{T^{5/2}}{\kappa_{latt}+\kappa_{bp}}. \quad (11)$$

Because the potentially high zT is determined by B factor, which is dependent on both the electronic properties, including m_d^* and U, and thermal properties, including κ_{latt} and κ_{bp}, the S substitution would be an effective way to improve the thermoelectric performance of Bi-Sb-Te alloys. The calculated B factor is shown in Fig. 7(b). Owing to the improved transport parameters, including m_d^*, U_{VB}, κ_{latt}, and κ_{bp}, the B factor of $Bi_{0.49}Cu_{0.01}Sb_{1.5}Te_{2.97}S_{0.03}$

was significantly enhanced by over 80 % as compared to that of the $Bi_{0.5}Sb_{1.5}Te_3$ within the entire measured temperature range.

If the favorable effect of the S substitution on the transport properties of Bi-Sb-Te alloys is maintained, zT can be further enhanced by the optimization of n_H. When acoustic phonon scattering is dominant [18], the maximum attainable zT is estimated with an optimum n_H using the B factor and the chemical potential (η) based on the following:

$$zT = \frac{S^2}{\frac{{k_B}^2}{e^2 B F_0(\eta)} + L}, \tag{12}$$

where $F_i(\eta)$ is the Fermi-Dirac integral with i^{th} order as below.

$$F_i(\eta) = \int_0^\infty \frac{x^i}{1+\exp(x-\eta)} dx. \tag{13}$$

Using the η-dependent S and L values (details are described in the Supplemental Information), zT as a function of n_H is estimated at different temperatures, as shown in Figs. 8(a)–(f). Although this estimation is conducted at a constant B factor, it is noted that zT_{max} and zT_{avg} could be simultaneously enhanced at $n_H \sim 2 \times 10^{19}$ cm^{-3}, which is easily attainable by additional compositional tuning.

4. Conclusions

In this study, we prepared S-substituted p-type $Bi_{0.49}Cu_{0.01}Sb_{1.5}Te_3$ in an effort to enhance the thermoelectric performance over a wide temperature range via the manipulation of deformation potential and band structure. The substitution of isovalent S at Te-site increases the density of states effective mass and weighted mobility of the valence band simultaneously by controlling the interaction between the phonons and carriers (both holes and electrons), which selectively activates the transport of holes. The power factor is improved within the entire measured temperature range (300 – 520 K) by the S substitution ($\leq$ 1 at.%). Additionally, the lattice thermal conductivity is reduced because of the intensified point-defect phonon scattering; bipolar thermal conductivity is also suppressed at higher temperatures by the activation of p-type conduction. Benefitting from this synergetic effect, the average value of zT between 300 and 520 K reaches above 1.0, which directly indicates the enhanced thermoelectric power generation efficiency.

Declaration of Competing Interest

The authors declare that they have no known competing financial interests or personal relationships that could have appeared to influence the work reported in this paper.

Acknowledgements

This research was supported by the Global Frontier Program through the Global Frontier Hybrid Interface Materials (GFHIM) project (Grant2013M3A6B1078870) and the Basic Science Research Program through the National Research Foundation of Korea (NRF) funded by the Ministry of Education (NRF-2019R1A6A1A11055660). This work was also supported by the Technology Innovation Program (20000149, Development of non-rare half-Heusler thermoelectric alloys for mid to high temperature waste heat recovery) funded By the Ministry of Trade, Industry & Energy (MOTIE, Korea).

Supplementary materials

Supplementary material associated with this article can be found, in the online version, at doi:10.1016/j.actamat.2020.116578.

References

[1] C. Haddard, Some efficient solutions to recover low and medium waste heat: competitiveness of the thermoacoustic technology, Energy Procedia 50 (2014) 1056.
[2] L.E. Bell, Cooling, heating, generating power, and recovering waste heat with thermoelectric systems, Science 321 (2008) 1457.
[3] K. Kim, G Kim, S.I. Kim, K.H. Lee, W. Lee, Clarification of electronic and thermal transport properties of Pb-, Ag-, and Cu-doped p-type $Bi_{0.52}Sb_{1.48}Te_3$, J. Alloys Compd. 772 (2019) 593.
[4] J.S. Yoon, J.M. Song, J.U. Rahman, S. Lee, W.S. Seo, K.H. Lee, S. Kim, H.S. Kim, S.I. Kim, W.H. Shin, High thermoelectric performance of melt-spun $Cu_xBi_{0.5}Sb_{1.5}Te_3$ by synergetic effect of carrier tuning and phonon engineering, Acta Mater 158 (2018) 289.
[5] H. Cho, H. Kim, M. Kim, K.H. Lee, S.W. Kim, S. Kim, Enhanced thermoelectric performance of Cu-incorporated $Bi_{0.5}Sb_{1.5}Te_3$ by melt spinning and spark plasma sintering, J. Electron. Mater. 49 (2020) 2789.
[6] H. Kim, K.H. Lee, J. Yoo, J. Youn, J.W. Roh, S. Kim, S.W. Kim, Effect of substitutional Pb doping on bipolar and lattice thermal conductivity in p-type $Bi_{0.48}Sb_{1.52}Te_3$, Materials 10 (2017) 763.
[7] J.L. Cui, H.F. Xue, W.J. Xiu, Microstructures and thermoelectric properties of p-type pseudo-binary $Ag_xBi_{0.5}Sb_{1.5-x}Te_3$ (x = 0.05–0.4) alloys prepared by cold pressing, Mater. Lett. 60 (2006) 3669.
[8] J.L. Cui, H.F. Xue, W.J. Xiu, W. Yang, X.B. Xu, Thermoelectric properties of Cu–doped p-type pseudo-binary $Cu_xBi_{0.5}Sb_{1.5-x}Te_3$ (x = 0.05–0.4) alloys prepared by spark plasma sintering, Scripta Mater 55 (2006) 371.
[9] H. Mun, K.H. Lee, S.J. Kim, J.-Y. Kim, J.H. Lee, J.-H. Lim, H.J. Park, J.W. Roh, S.W. Kim, Fe-doping effect on thermoelectric properties of p-type $Bi_{0.48}Sb_{1.52}Te_3$, Materials 8 (2015) 959.
[10] H.S. Kim, S. Choo, H. Cho, S. Kim, Beneficial influence of Co-doping on thermoelectric efficiency with respect to electronic and thermal transport properties, Phys. Status Solidi a 216 (2019) 1900039.
[11] H.-S. Kim, K.H. Lee, J. Yoo, W.H. Shin, J.W. Roh, J.-Y. Hwang, S.W. Kim, S.-I. Kim, Suppression of bipolar conduction via bandgap engineering for enhanced thermoelectric performance of p-type $Bi_{0.4}Sb_{1.6}Te_3$ alloys, J. Alloy Compd. 741 (2018) 869.
[12] K.H. Lee, S.M. Choi, J.W. Roh, S.W. Hwang, S.I. Kim, W.H. Shin, H.J. Park, J.H. Lee, S.W. Kim, D.J. Yang, Enhanced thermoelectric performance of p-type Bi-Sb-Te alloys by codoping with Ga and Ag, J. Electron. Mater. 44 (2015) 1531.
[13] Z.G. Chen, G. Han, L. Yang, L. Cheng, J. Zou, Nanostructured thermoelectric materials: Current research and future challenge, Prog. Nat. Sci. 22 (2012) 535.
[14] J.F. Li, W.S. Liu, L.D. Zhao, M. Zhou, High-performance nanostructured thermoelectric materials, NPG Asia Mater 2 (2010) 152.
[15] A.J. Minnich, M.S. Dresselhaus, Z.F. Ren, G. Chen, Bulk nanostructured thermoelectric materials: current research and future prospects, Energy Environ. Sci. 2 (2009) 466.
[16] B. Poudel, Q. Hao, Y. Ma, Y. Lan, A. Minnich, B. Yu, X. Yan, D. Wang, A. Muto, D. Vashaee, X. Chen, J. Liu, M.S. Dresselhaus, G. Chen, Z. Ren, High-thermoelectric performance of nanostructured bismuth antimony telluride bulk alloys, Science 320 (2008) 5876.
[17] F.K. Lotgering, Topotactical reactions with ferrimagnetic oxides having hexagonal crystal structures–I, J. Inorg. Nucl. Chem. 9 (1959) 113.
[18] A.F. May, G.J. Snyder, D.M. Rowe (Ed.), CRC Press, Boca Raton, 2012.
[19] Y. Pei, H. Wang, G.J. Snyder, Band engineering of thermoelectric materials, Adv. Mater. 24 (2012) 6125.
[20] R.P. Chasmar, R. Stratton, The thermoelectric figure of merit and its relation to thermoelectric generators, J. Electronics and Control 7 (1959) 52.